analytical chemistry

ARTICLE

pubs.acs.org/ac

Surface Plasmon Resonance Phase Imaging Measurements of Patterned Monolayers and DNA Adsorption onto Microarrays

Aaron R. Halpern,[†] Yulin Chen,[†] Robert M. Corn,[†] and Donghyun Kim[*,†,‡]

[†]Department of Chemistry, University of California at Irvine, Irvine, California 92697, United States

[‡]School of Electrical and Electronic Engineering, Yonsei University, Seoul, Korea 120-749

ABSTRACT: The optical technique of surface plasmon resonance phase imaging (SPR-PI) is implemented in a linear microarray format for real-time measurements of surface bioaffinity adsorption processes. SPR-PI measures the phase shift of *p*-polarized light incident at the SPR angle reflected from a gold thin film in an ATR Kretschmann geometry by creating an interference fringe image on the interface with a polarizer−quartz wedge depolarizer combination. The position of the fringe pattern in this image changes upon the adsorption of biomolecules to the gold thin film. By using a linear array of 500 μm biosensor element lines that are perpendicular to the interference fringe image, multiple bioaffinity adsorption measurements can be performed in real time. Two experiments were performed to characterize the sensitivity of the SPR-PI measurement technique: First, a ten line pattern of a self-assembled monolayer of 11-mercaptoundecamine (MUAM) was created via photopatterning to verify that multiple phase shifts could be measured simultaneously. A phase shift difference ($\Delta\phi$) of $\Delta\phi = 182.08 \pm 0.03°$ was observed for the 1.8 nm MUAM monolayer; this value agrees with the phase shift difference calculated from a combination of Fresnel equations and Jones matrices for the depolarizer. In a second demonstration experiment, the feasibility of SPR-PI for in situ bioaffinity adsorption measurements was confirmed by detecting the hybridization and adsorption of single stranded DNA (ssDNA) onto a six-component DNA line microarray patterned monolayer. Adsorption of a full DNA monolayer produced a phase shift difference of $\Delta\phi = 28.80 \pm 0.03°$ at the SPR angle of incidence and the adsorption of the ssDNA was monitored in real time with the SPR-PI. These initial results suggest that SPR-PI should have a detection limit roughly 100 times lower than traditional intensity-based SPR imaging measurements.

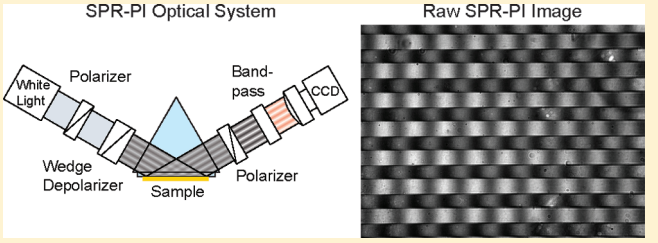

Surface plasmon resonance (SPR) methods are optical techniques that exploit the sensitivity of surface plasmon polaritons (SPPs) created at a metal−dielectric interface to the local index of refraction for the measurement of interfacial adsorption and thin film deposition processes.[1] SPR has become an extremely useful technique for obtaining quantitative real-time kinetic information on surface bioaffinity interactions and has been implemented in many forms for biosensing applications.[2,3] The sensitivity of SPR methods to any local refractive index change make them universally applicable to all bioaffinity adsorption events, but at the loss of biomolecular selectivity. This selectivity limitation can be overcome by using SPR in a high throughput, multiplexed format to simultaneously monitor multiple bioaffinity adsorption processes onto a variety of microarray elements. SPR imaging (SPRI) methods are an example of such a multiplexed SPR measurement that has been widely applied to many types of bioaffinity sensing applications.[4−6]

A second issue with SPR methods has been the inherent sensitivity of the method for the detection of bioaffinity adsorption processes. The SPR technique works best for detecting larger molecules (e.g., proteins, antibodies), typically at concentrations of 100 pM or higher. In comparison, typical fluorescence imaging measurements are limited by background fluorescence to a typical detection limit of 1−10 pM[7,8] and will work with any molecule provided that it contains a fluorophore. Sandwich-based bioaffinity measurements that use a metal, polymer, or silica nanoparticle have been used to lower the SPR detection limit to 1−10 pM,[9−12] and other surface plasmonic nanostructured surfaces have been recently suggested as alternatives to SPR methods with sensitivities even down to femtomolar concentrations.[13−17] Most of these new techniques, however, have not yet been implemented in a multiplexed or microarray format.

One successful method for improving the sensitivity of SPR measurements that does not require changes in surface structure or the addition of nanoparticles is the replacement of the measurement of the **intensity** of reflected light with the measurement of **phase** of the reflected light. SPPs cannot be created on isolated planar metal−dielectric interfaces; instead, SPPs are typically injected onto a metal−dielectric interface by coupling to a *p*-polarized photon incident on a prism/thin-film/dielectric configuration known as the Kretchsmann geometry. At the SPR angle, the incident *p*-polarized photons have a momentum in the surface plane that matches the momentum of SPPs at that wavelength. A large dip in reflectivity is observed at the SPR

Received: January 19, 2011
Accepted: February 3, 2011
Published: February 28, 2011

angle, as shown in the theoretical reflectivity curve shown in Figure 1. Changes in the position of the SPR angle as measured by reflectivity are the basis for many SPR measurements; other measurements such as SPRI detect the concomitant changes in reflectivity near the SPR angle upon adsorption. An alternative method is to measure the Fresnel phase shift of the *p*-polarized reflected light at the SPR angle, δ_p. This phase shift is the argument of the complex Fresnel reflection coefficient.[18] As shown in Figure 1, for *p*-polarized light there is a very sharp (maximum) phase shift of 2π or 360° in the region of the SPR angle, relative to the phase shift at the critical angle. Changes in this phase shift upon adsorption have been used in various optical configurations as a highly sensitive method of monitoring surface adsorption processes,[19−23] with detection limits up to two orders of magnitude lower than amplitude detection approaches.[24,25]

In this paper, we explore the use of SPR phase measurements in a microarray format, SPR phase imaging (SPR-PI), for the simultaneous real time measurement of multiple bioaffinity adsorption processes. Phase-sensitive SPR detection methods have been implemented previously in both a single channel and multiplexed format.[26] Most phase-sensitive SPR methods use a Mach−Zehnder interferometer with lock-in detection,[24,27,28] but a few have demonstrated the use of interference fringes created on the gold thin film.[29,30] Our implementation of SPR-PI is shown in Figure 2a. A variable retarder creates a spatially periodic retardation pattern on the metal interface as shown in Figure 2b; this periodic polarization state is converted into a fringe pattern by a subsequent linear polarizer (see Figure 2c). The position of the interference fringes defines a phase shift ϕ that is related to δ_p as shown in the Appendix. A change in the phase shift, denoted as a phase shift difference, ($\Delta\phi$) is tracked in real time and used to monitor any phase shift changes due to a molecular adsorption. Two experiments were performed to characterize the sensitivity of the SPR-PI measurement technique; first, a pattern of an alkanethiol self-assembled monolayer was created via photopatterning to verify that multiple phase shift differences could be measured simultaneously, and second, the feasibility of SPR-PI for in situ bioaffinity adsorption measurements was confirmed by detecting the hybridization and adsorption of single stranded DNA (ssDNA) onto a six component DNA line microarray patterned monolayer.

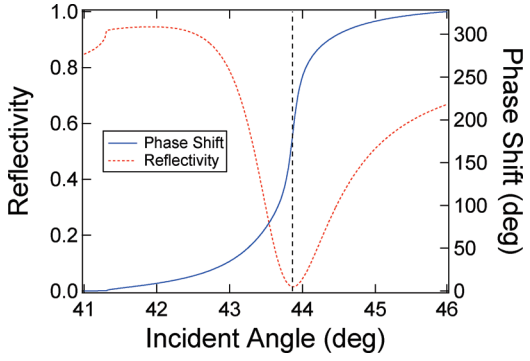

Figure 1. Theoretical reflectivity (R_p) and Fresnel phase shift (δ_p) curves for a 45 nm Au thin film on a BK7 substrate plotted as a function of incident angle θ. These curves were calculated with a three-layer Fresnel calculation. The dotted vertical line represents the SPR angle, θ_{SPR}. A very large phase shift of 2π is observed at the SPR angle.

METHODS AND MATERIALS

Sample Fabrication. Planar Au films (45 nm thick) were thermally evaporated onto cleaned BK7 glass slides (Schott, Duryea, PA, USA) with a 1 nm Cr adhesion layer. For in situ SPR phase chips, cleaned SF10 glass slides were silanized with Sigmacote (Sigma, St. Louis, MO, USA) using the protocol provided by the manufacturer. A shadow mask was then used to deposit 1 mm wide Au stripes (45 nm thick) with a 1.5 mm period onto the SF10 glass slides (Schott) with a 1 nm Cr adhesion layer.

Surface Chemistry. For a photopatterned 11-mercaptoundecamine monolayer (MUAM), the planar Au slides were immersed in an ethanolic 1 mM MUAM solution (Dojindo, Rockville, MD, USA) overnight. After rinsing with ethanol and drying with a stream of N_2, the slides were exposed to UV light from a 1000-W Xe arc lamp (Oriel, Irvine, CA, USA) behind a Cr photomask (0.5 mm Cr bars with 1 mm period) for 30 min, as shown in Figure 3a. This was followed by rinsing with water and

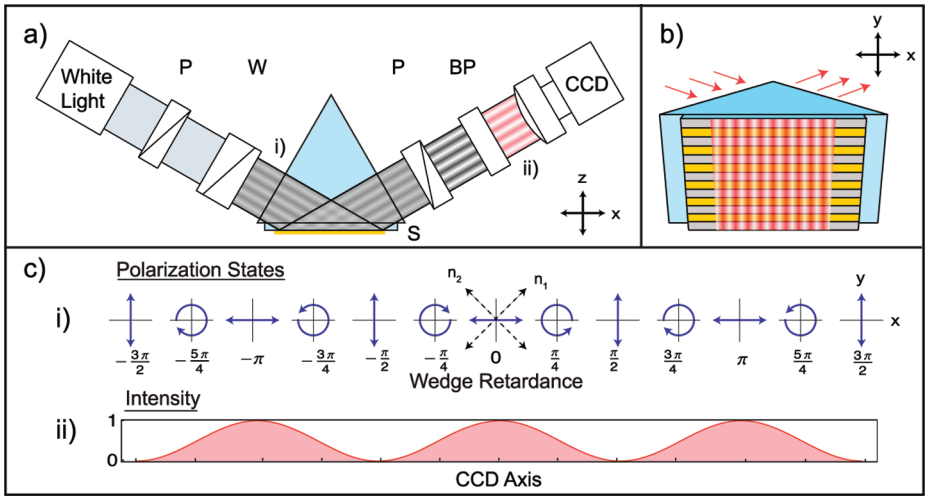

Figure 2. (a) Optical configuration for SPR-PI: (P) polarizer, (W) wedge retardance plate, and (BP) bandpass filter. (b) Schematic diagram of the sample chip. Horizontal Au stripes represent sample areas with different biointeractions, while red vertical patterns are the sinusoidal phase fringes. (c) Schematic diagrams of (i) polarization states before prism corresponding to wedge retardance values δ_x as detailed in the Appendix and (ii) spatial intensity distribution at CCD disregarding prism−substrate phase retardance.

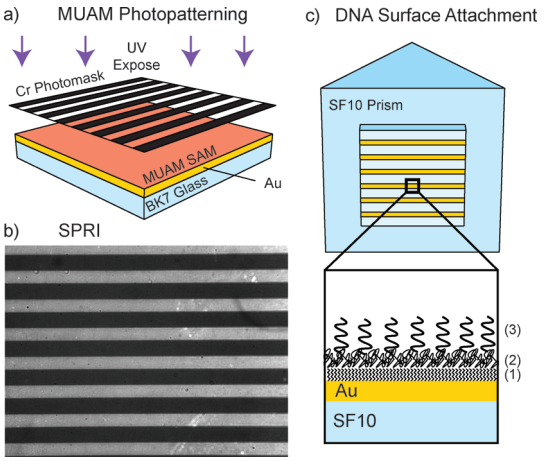

Figure 3. Surface chemistry and sample fabrication schematics: (a) MUAM photopatterning procedure, (b) SPRI image of photopatterned MUAM, and (c) SPR-PI sample line array and DNA surface attachment chemistry shown stepwise as (1) formation of a MUAM monolayer, (2) electrostatic adsorption of pGlu, and (3) simultaneous EDC/NHSS coupling of DNA to pGlu and pGlu to MUAM.

drying with N_2. The photopatterned slides were immediately coupled to a right angle BK7 prism for imaging. Figure 3b shows an SPR image experimentally obtained at an incident angle θ = 43.73°. At this incident angle, the bare substrate without MUAM is at resonance while the stripes with MUAM are off resonance.

The surface chemistry for DNA attachment is illustrated in Figure 3c. First, the SPR phase chips were immersed in an ethanolic 1 mM MUAM solution overnight, followed by rinsing with ethanol and drying with N_2 (1). The Au surfaces were covered in a 2 mg/mL solution of poly-L-glutamic acid sodium salt (pGlu, Sigma, St. Louis, MO, USA, MW 50−100 kD) in buffer (10 mM Na_2HPO_4, 137 mM NaCl, 2.7 mM KCl_2, pH 7.4) for 1 h (2). The Au stripes were then spotted with a 250 μM ssDNA solution (5′ amino-modified A_{25} or T_{30}) containing 75 mM 1-ethyl-3-(3-(dimethylamino)propyl)carbodiimide hydrochloride (EDC, Pierce, Rockford, IL, USA) and 15 mM *N*-hydroxysulfosuccinimide (NHSS, Pierce) in buffer and allowed to react for 4 h (3). Rinsing with water and gently drying with N_2 followed each step. Detailed pGlu attachment procedures are described elsewhere.[31] For DNA hybridization phase measurements, a 1 μM complementary ssDNA solution was flowed into an in situ SPR imaging flow cell and phase images were recorded at the SPR resonance angle.

Optical Setup. Our SPR-PI has been set up following the configuration described in Figure 2a. The SPR sensing system was constructed for phase detection using white light from a tungsten lamp as a light source and a charge-coupled device (CCD, QICAM, Qimaging, Surrey, BC, Canada) as a photodetector array. The incident light is collimated and *p*-polarized as it passes through a wedge depolarizer (W, no. 80-1015-633, Special Optics Inc., Wharton, NJ, USA) to form periodically varying polarization states (represented as low contrast fringes in Figure 2ai and shown explicitly in Figure 2ci). The depolarizer consists of a pair of quartz wedges that are optically in contact. The fast axes of the prisms are aligned to be 90° apart and 45° with respect to the *x*-axis (as shown as the dotted lines labeled n_1 and n_2 in Figure 2ci, where the *x*-axis corresponds to *p*-polarized light). An SF10 equilateral prism, where a sample (S) is optically coupled with index matching oil (Cargille Laboratories, Cedar Grove, NJ, USA), is mounted on a motorized rotation stage for adjusting the angle of light incidence (θ). The light out of the prism is then passed through a linear polarizer slightly off the *x*-axis (∼2°) to create a fringe pattern (represented as high contrast fringes in Figure 2aii and shown as it appears in the CCD in Figure 2cii) associated with *p* and *s* polarization components and finally a 633 ± 10 nm optical bandpass filter (BP) before being collected by the CCD. Note that Figure 2cii disregards all additional phase shift given by the prism sample due to SPR. The whole operation is computer-controlled by LabView. Traditional angle-scanning SPR detection was performed simply by removing the depolarizer from the SPR-PI setup.

RESULTS AND DISCUSSION

SPR-PI Measurements of Photopatterned MUAM Monolayers. In a first set of experiments, we obtained and analyzed SPR-PI phase images from a line array pattern of a self-assembled MUAM monolayer. The images were obtained from samples containing alternating stripes of a bare gold substrate and MUAM that were created by a photopatterning process shown schematically in Figure 3a. Figure 3b shows the normal SPRI image of the test line array; the bright stripes correspond to the areas of the gold surface that are modified with the MUAM monolayer, and the dark stripes are from areas of bare gold surface.

A series of phase shift images were obtained at an incident angles (θ) ranging from θ = 41° to 46° at 0.02° intervals. Figure 4a shows the phase image obtained at an incident angle of θ = 43.86° ± 0.02°; this phase image exhibited the maximum phase shift difference between the MUAM-modified gold surface and the bare gold surface. This phase shift difference ($\Delta\phi$) was quantified by first 2D Fourier filtering the image (Figure 4b) and then creating two sine wave functions from the filtered image (Figure 4c). The sine waves in Figure 4c were obtained from the two regions (blue = bare gold, red = MUAM) of the Fourier filtered image. Using these two sine waves, a phase shift difference of $\Delta\phi$ = 182.0 ± 0.03° was measured.

The phase shift difference ($\Delta\phi$ = black curve) for all incident angles from θ = 41° to 46° is plotted in Figure 5. This data exhibits a narrow peak (fwhm of $\Delta\theta$ = 0.31°) in the region of the SPR angle (θ_{SPR} = 43.86 ± 0.02°) denoted as angle A in the Figure. Note that this angle differs from the angle at which conventional SPR imaging measurements are performed (denoted as angle B). Also shown in Figure 5 are the SPR reflectivity curves for the lines of MUAM-modified gold surface (red curve) and the lines of bare gold surface (blue curve) that were extracted from SPRI image data. The maximum in $\Delta\phi$ = 182° occurred in between the SPR angle for the bare gold surface (θ_{SPR} = 43.73°) and the MUAM-modified gold surface (θ_{SPR} = 43.93°).

The phase shift difference data obtained from the SPR-PI images can be compared with phase shift difference obtained from Fresnel calculations. Figure 6 shows a plot of both phase shift difference and reflectivity calculations; these intensity and phase characteristics are obtained using a combination of Fresnel equations and Jones calculus as described in the Appendix. This combined calculation is required to correctly describe the phase patterns created by the wedge depolarizer. The theoretical curves vary slightly from the experimental data ($\Delta\phi_{max}$ = 186° instead of 182° and the fwhm is $\Delta\theta$ = 0.35° instead of $\Delta\theta$ = 0.31°); we attribute these differences to a combination of experimental artifacts (e.g., incomplete collimation of the incident beam, beam

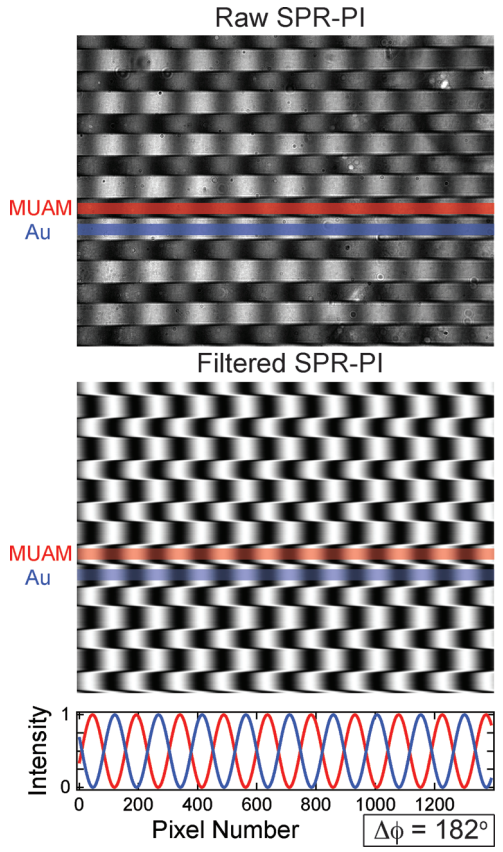

Figure 4. SPR-PI images and phase extraction procedure: (a) SPR-PI image showing maximum phase shift difference ($\Delta\phi$) of patterned MUAM monolayer at an incidence angle of θ = 43.86°, (b) Fourier filtered SPR-PI image from part a, and (c) two sine waves generated from part b showing maximum phase shift difference measured to be $\Delta\phi_{max}$ = 182° between the bare gold surface (blue) and MUAM-modified gold surface (red).

walk) and limitations of the theory (e.g., approximate indices of refraction for the MUAM monolayer).

From these measurements, the sensitivity of SPR-PI can be compared to conventional SPR imaging methods. Conventional SPR imaging yields a reflectivity difference ($\Delta\%R$) of 11.9% between the two surfaces. Given that the minimum detectable change in reflectivity is approximately 0.2%,[31] we calculate that changes as small as approximately 2% of a full MUAM monolayer is detectable. In comparison to SPRI, with SPR-PI we observe a 182° maximum phase shift difference for a MUAM monolayer, and we can detect a phase difference as small as $\Delta\phi$ = 0.03°. Thus, with SPR-PI we should be able to detect ~0.02% of a MUAM monolayer, which is a 100× improvement in sensitivity. This calculation confirms our expectation that SPR-PI should have an improved sensitivity as compared to intensity-based SPR imaging.

SPR-PI Measurements of DNA Hybridization Adsorption onto DNA Line Arrays. The measurements on MUAM monolayers do not predict the limit of detection for SPR-PI in terms of the lowest concentration that can be measured; for that number, we need to perform experiments on the bioaffinity adsorption of a particular analyte, such as single-stranded DNA (ssDNA) onto a ssDNA microarray. To quantitatively ascertain the biosensing capabilities of SPR-PI measurements, we have monitored in situ the hybridization adsorption of ssDNA onto a two-component ssDNA line array.

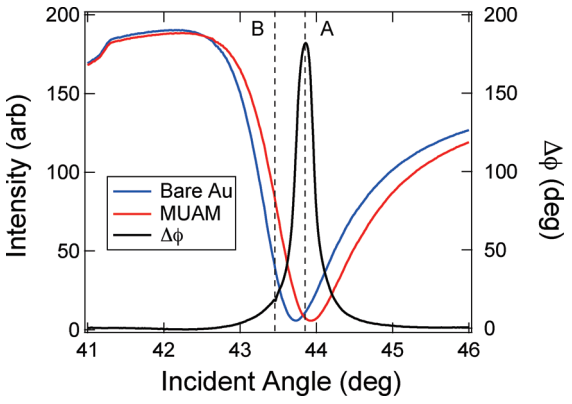

Figure 5. Observed phase shift difference and reflectivity curves for the bare gold and MUAM-modified gold regions (as depicted in Figure 4) obtained from a series of SPRI and SPR-PI measurements as a function of incident angle. The phase shift difference between the two surfaces ($\Delta\phi$) is plotted as the black curve. The reflectivity curves corresponding to the bare gold surface and MUAM-modified gold surface are plotted as the blue and red curves, respectively. The incident angle at the dotted line marked A denotes the angle of incidence, $\theta_{SPR\text{-}PI}$, with maximum phase shift difference that should be used for SPR-PI measurements, whereas B denotes the angle that exhibits the maximum reflectivity change $\Delta\%R$, used for SPRI.

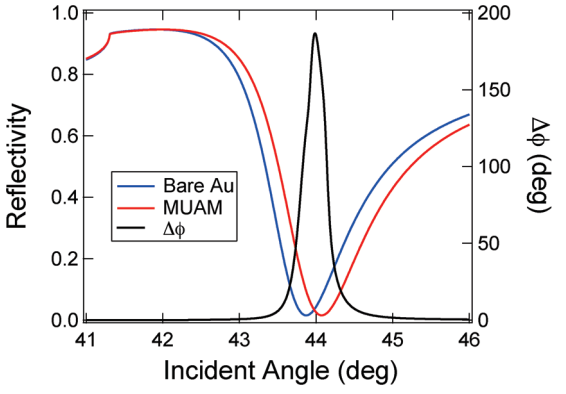

Figure 6. Calculated phase shift difference (black) between bare gold and MUAM-modified gold using a combination of Fresnel equations and Jones calculus. Also shown in the figure are the reflectivity curves calculated from Fresnel equations for the two surfaces. Reflectivity curves corresponding to the bare gold surface and MUAM-modified gold surface are plotted as the blue and red curves, respectively. The data are very consistent with experimental curves presented in Figure 5.

The process for fabricating this line array is shown in Figure 3b. A pattern of gold lines (1 mm) were vapor-deposited through a mask onto an SF10 glass substrate. These gold lines were then modified with MUAM, and then ssDNA was attached to the lines using a two-step polyelectrolyte (poly-L-glutamic acid) adsorption/EDC:NHSS coupling reaction of amino-modified ssDNA that we have described previously.[31] Six alternating lines of ssDNA with sequences A_{25} and T_{30} were created. This line array was then sealed into a microfluidic chamber (total volume: 40 μL) for the in situ SPR-PI measurements.

The ssDNA array was then exposed to a ssDNA target solution that contained 1.0 μM A_{25} ssDNA; the real-time adsorption kinetics data are shown in Figure 7. Phase images are obtained at 5 s intervals, and then, the phase of the various ssDNA line

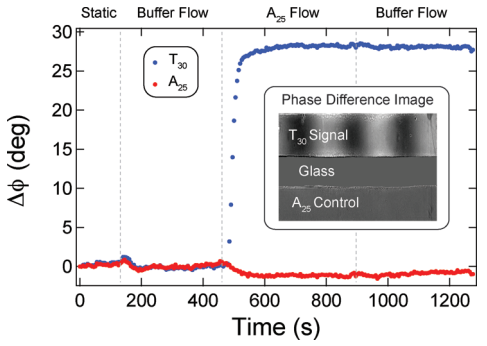

Figure 7. Real-time SPR-PI measurements of the phase shift difference, $\Delta\phi$ observed upon adsorption of DNA onto a two-component DNA microarray. Phase shift difference data from the in situ DNA hybridization adsorption of ssDNA (sequence A_{25}, 1 μM solution) onto a T_{30} ssDNA array element and a A_{25} sDNA array elements are shown as the blue and red circles, respectively. Time points denoted on the graph with vertical dotted lines are for the commencement of microfluidic buffer flow (135 s), the introduction of the target ssDNA solution (425 s), and the reintroduction of a buffer solution (900 s). Composite phase difference image for the two array elements created from SPR-PI data before and after hybridization adsorption are shown in the inset to the figure.

elements is extracted using the data analysis process described above. The blue dots in the figure are the phase shift difference data from a T_{30} element, and the red dots are the phase shift difference data from a neighboring A_{25} element. The ssDNA from solution only adsorbs to the T_{30} elements, indicating a specific adsorption process due to hybridization (we term this "hybridization adsorption"). As expected, no phase shift difference for the hybridization adsorption of A_{25} onto the A_{25} control array elements was observed. The adsorption of A_{25} onto the T_{30} array produced a phase shift difference of $\Delta\phi = 28.80 \pm 0.03°$. Because we are at a concentration of 1 μM, this corresponds to the phase shift difference for the adsorption of a full monolayer onto the surface.

To visualize this phase shift difference, a two line composite difference image is displayed in the inset of Figure 7. This image was generated by subtracting two intervals of summed images from 250 to 450 and 550 to 750 s, corresponding to before and after hybridization. A sinusoidal fringe pattern appears in the top region of the difference image on the T_{30} modified surface indicating a phase shift difference; however, the stationary pattern on the A_{25} control cancels itself out in the before and after image so that no pattern appears in the bottom region.

This phase shift difference of $\Delta\phi = 28.80°$ for a full monolayer can be used to compare the sensitivity of the SPR-PI with conventional SPR imaging measurements. If again we assume a minimum detectable phase shift difference of $\Delta\phi = 0.03°$, we predict that we should be able to measure 0.1% of a DNA monolayer. At low concentrations, the surface coverage Γ is linearly proportional to the solution concentration and the Langmuir adsorption coefficient, K_{ads} ($\Gamma/\Gamma_{max} = K_{ads}C$). Since the Langmuir adsorption coefficient for ssDNA adsorption is approximately $2 \times 10^7\ M^{-1}$, this corresponds to a concentration detection limit of 50 pM ($C_{lod} = 0.001/(2 \times 10^7)$). In our previous work using conventional SPRI measurements, we have reported that the hybridization adsorption of ssDNA onto DNA microarrays yields an SPRI reflectivity change $\Delta\%R$ of 2.4% for a full monolayer, with a minimum detectable $\Delta\%R$ of 0.2%, corresponding to 8% of a monolayer, or a concentration detection limit C_{lod} of ~5 nM ($= 0.08/(2 \times 10^7)$).[31] Thus we find again that the SPR-PI measurements are approximately 100 times more sensitive than the SPRI measurements.

CONCLUDING REMARKS

In summary, we have used SPR-PI for characterization of MUAM formation ex situ and DNA hybridization in situ as biosensing targets. The results suggest that SPR-PI should provide dynamic range that is comparable to conventional intensity based SPR techniques and yet detection sensitivity much superior by two orders of magnitude. As an imaging technique, we expect that SPR-PI can allow high-throughput in situ monitoring of molecular events at much improved detection sensitivity that would not be available in conventional SPR imaging configurations.

APPENDIX

Jones Calculus of SPR-PI Model. In these SPR-PI measurements, we measure the phase shift difference $\Delta\phi$ for the different microarray elements. The observed phase shift difference in our experimental apparatus can be described by the combination of Fresnel equations and Jones calculus.

The polarization states of light in the SPR-PI set-up can be understood in terms of Jones calculus. The Jones vector for the output light is given as

$$J_{out} = \mathbf{M}(LP_{out})\mathbf{M}(SPR)\mathbf{M}(W)\mathbf{M}(LP_{in})J_{in} \quad (A.1)$$

where J_{in} and J_{out} are Jones matrices for input and output light. $\mathbf{M}$ denotes the Jones matrix associated with each polarization component. Following the path of the light (moving from right to left in A.1), the Jones vector for the incident light after an initial linear polarizer is represented as

$$\mathbf{M}(LP_{in})J_{in} = \begin{bmatrix} 1 \\ 0 \end{bmatrix} \quad (A.2)$$

Next, the Jones matrix for the wedge depolarizer can be described as

$$\mathbf{M}(W) = \begin{bmatrix} \cos\psi_W & -\sin\psi_W \\ \sin\psi_W & \cos\psi_W \end{bmatrix} \begin{bmatrix} e^{i\delta_x} & 0 \\ 0 & 1 \end{bmatrix} \begin{bmatrix} \cos\psi_W & \sin\psi_W \\ -\sin\psi_W & \cos\psi_W \end{bmatrix} \quad (A.3)$$

where ψ_W establishes the orientation of the optical axes, set as 45° in this case with application of the rotation matrix. Note that in general, the phase retardance given by the wedge can be a spatially varying function that depends on the thicknesses and birefringence of the two wedges in the depolarizer; however, here we only consider a linearly varying retardance, δ_x, along the x-axis for simplicity. The wedge creates light incident on the prism substrate having periodically varying polarization states as depicted in Figure 2ci. Since SPR can be described by

$$\mathbf{M}(SPR) = \begin{bmatrix} R_p e^{i\delta_p} & 0 \\ 0 & R_s e^{i\delta_s} \end{bmatrix} \quad (A.4)$$

where R_p and R_s are Fresnel reflection coefficients and δ_p and δ_s are Fresnel phase shifts that accompany SPR for p and s polarizations, respectively. The effect of SPR, as far as Jones calculus is

dx.doi.org/10.1021/ac200157p |Anal. Chem. 2011, 83, 2801–2806

concerned, is to make an additional contribution to the retardance that also depends on the ratio of p to s.

The output after the prism still contains periodically varying polarization states. Only after being passed through the output polarizer in front of a CCD are the intensity fringes characteristic of SPR-PI formed. The Jones vector of the light at the output detected by CCD can be evaluated after being passed through the final linear polarizer

$$\mathbf{M}(\mathrm{LP}_{\mathrm{out}}) = \begin{bmatrix} \cos\psi_{\mathrm{lp}} & -\sin\psi_{\mathrm{lp}} \\ \sin\psi_{\mathrm{lp}} & \cos\psi_{\mathrm{lp}} \end{bmatrix} \begin{bmatrix} 1 & 0 \\ 0 & 0 \end{bmatrix} \begin{bmatrix} \cos\psi_{\mathrm{lp}} & \sin\psi_{\mathrm{lp}} \\ -\sin\psi_{\mathrm{lp}} & \cos\psi_{\mathrm{lp}} \end{bmatrix} \tag{A.5}$$

where ψ_{lp} is small ($\sim 2°$). The intensity detected by the CCD will then take the form of

$$I_{\mathrm{out}} = J_{\mathrm{out}} J_{\mathrm{out}}^{*} \tag{A.6}$$

and results in a oscillatory intensity pattern. These equations were used to calculate the pattern shown in Figure 2b (note that, in this figure, the additional phase retardance contributed by the prism substrate has been disregarded by omitting $\mathbf{M}$(SPR)). The frequency of the oscillatory pattern depends on the rate of change of δ_x across the wedge depolarizer. The phase of this oscillatory pattern, ϕ, is defined by the position of the maxima in the CCD image and depends upon the value of δ_p, R_p, δ_s, and R_s for a given angle incidence. In the MUAM photopatterning experiment, we measure the phase shift difference, $\Delta\phi$, between the bare and MUAM-modified gold surfaces at a given incident angle. This phase shift difference was also calculated using these equations and is shown in Figure 6. For the real time DNA hybridization adsorption experiments, we measure the phase shift difference $\Delta\phi$ observed for the two DNA microarray elements as a function of time during the measurement. The angle of incidence for this experiment is fixed at the SPR angle at the beginning of the experiment.

■ ACKNOWLEDGMENT

This research was supported by the National Institutes of Health (GM059622) and the National Science Foundation (CHE-0551935). D.K. was supported by the LG Yonam Foundation through LG Yonam Overseas Faculty Research Fellowship and, in part, by the National Research Foundation (NRF) of Korea through NRF 2009-0070732 and 2010-0007993.

■ REFERENCES

(1) Raether, H. *Surface Plasmons on Smooth and Rough Surfaces and on Gratings*; Springer: Berlin, 1988; Chapter 2.
(2) Liedberg, B.; Nylander, C.; Lunström, I. *Sens. Actuators* **1983**, *4*, 299–304.
(3) Schasfoort, R. B. M., Tudos, A. J., Eds. *Handbook of Surface Plasmon Resonance*; The Royal Society of Chemistry: Cambridge, 2008.
(4) Jordan, C. E.; Corn, R. M. *Anal. Chem.* **1997**, *69*, 1449–1456.
(5) Brockman, J. M.; Frutos, A. G.; Corn, R. M. *J. Am. Chem. Soc.* **1999**, *121*, 8044–8051.
(6) Brockman, J. M.; Nelson, B. P.; Corn, R. M. *Annu. Rev. Phys. Chem.* **2003**, *51*, 41–63.
(7) Nakatani, K.; Sando, S.; Saito, I. *Nat. Biotechnol.* **2001**, *19*, 51–55.
(8) Peterson, A. W.; Wolf, L. K.; Georgiadis, R. M. *J. Am. Chem. Soc.* **2002**, *124*, 14601–14607.
(9) He, L.; Musick, M. D.; Nicewarner, S. R.; Salinas, F. G.; Benkovic, S. J.; Natan, M. J.; Keating, C. D. *J. Am. Chem. Soc.* **2000**, *122*, 9071–9077.
(10) Sun, Y. G.; Xia, Y. N. *Anal. Chem.* **2002**, *74*, 5297–5305.
(11) Anker, J. N.; Hall, W. P.; Lyandres, O.; Shah, N. C.; Zhao, J.; Van Duyne, R. P. *Nat. Mater.* **2008**, *7*, 442–463.
(12) Sendroiu, I. E.; Warner, M. E.; Corn, R. M. *Langmuir* **2009**, *25*, 11282–11284.
(13) Kim, D. *J. Opt. Soc. Am. A* **2006**, *23*, 2307–2314.
(14) Kim, K.; Yoon, S. J.; Kim, D. *Opt. Express* **2006**, *14*, 12419–12431.
(15) Byun, K. M.; Yoon, S. J.; Kim, D.; Kim, S. J. *Opt. Lett.* **2007**, *32*, 1902–1904.
(16) Malic, L.; Cui, B.; Veres, T.; Tabrizian, M. *Opt. Lett.* **2007**, *32*, 3092–3094.
(17) Ma, K.; Kim, D. J.; Kim, K.; Moon, S.; Kim, D. *IEEE J. Sel. Topics Quant. Electron.* **2010**, *16*, 1004–1014.
(18) Hansen, W. N. *J. Opt. Soc. Am.* **1968**, *58*, 380–390.
(19) Nelson, S. G.; Johnston, K. S.; Yee, S. S. *Sens. Actuators B* **1996**, *35*, 187–191.
(20) Wu, S. Y.; Ho, H. P.; Law, W. C.; Lin, C.; Kong, S. K. *Opt. Lett.* **2004**, *29*, 2378–2380.
(21) Li, Y.-C.; Chang, Y.-F.; Su, L.-C.; Chou, C. *Anal. Chem.* **2008**, *80*, 5590–5595.
(22) Chiang, H.-P.; Lin, J.-L.; Chang, R.; Su, S.-Y.; Leung, P. T. *Opt. Lett.* **2005**, *30*, 2727–2729.
(23) Patskovsky, S.; Vallieres, M.; Maisonneuve, M.; Song, I.-H.; Meunier, M.; Kabashin, A. V. *Opt. Express* **2009**, *17*, 2255–2263.
(24) Kabashin, A. V.; Patskovsky, S.; Grigorenko, A. N. *Opt. Express* **2009**, *17*, 21191–21204.
(25) Su, Y.-D.; Chiu, K.-C.; Chang, N.-S.; Wu, H.-L.; Chen, S.-J. *Opt. Express* **2010**, *18*, 20125–20135.
(26) Chen, S.-J.; Su, Y.-D.; Hsiu, F.-M.; Tsou, C.-Y.; Chen, Y.-K. *J. Biomed. Opt.* **2005**, *10*, 034005.
(27) Notcovich, A. G.; Zhuk, V.; Lipson, S. G. *Appl. Phys. Lett.* **2000**, *76*, 1665–1667.
(28) Nikitin, P. I.; Grigorenko, A. N.; Beloglazov, A. A.; Valeiko, M. V.; Savchuk, A. I.; Savchuk, O. A.; Steiner, G.; Huebner, A.; Salzer, R. *Sens. Actuators A* **2000**, *85*, 189–193.
(29) Wong, C. L.; Ho, H. P.; Suen, Y. K.; Kong, S. K.; Chen, Q. L.; Yuan, W.; Wu, S. Y. *Biosens. Bioelectron.* **2008**, *24*, 606–612.
(30) Yu, X.; Ding, X.; Liu, F.; Wei, X.; Wang, D. *Meas. Sci. Technol.* **2008**, *19*, 015301.
(31) Chen, Y.; Nguyen, A.; Niu, L.; Corn, R. M. *Langmuir* **2009**, *25*, 5054–5060.